ChemComm

COMMUNICATION

View Article Online
View Journal

Cite this: DOI: 10.1039/d1cc02396a

Received 6th May 2021,
Accepted 1st June 2021

DOI: 10.1039/d1cc02396a

rsc.li/chemcomm

A star-shaped cyclopentadithiophene-based dopant-free hole-transport material for high-performance perovskite solar cells†

Kun-Mu Lee,[abc] Jui-Yu Yang,[d] Ping-Sheng Lai,[e] Ke-Jyun Luo,[d] Ting-Yu Yang,[d] Kang-Ling Liau,[f] Seid Yimer Abate [g] and Yan-Duo Lin *[d]

A new cyclopentadithiophene (CPDT)-based organic small molecule serves as an efficient dopant-free hole transport material (HTM) for perovskite solar cells (PSCs). Upon incorporation of two carbazole groups, the resulting CPDT-based HTM (C-CPDT) shows an impressive power conversion efficiency (PCE) of 19.68% with better stability compared with those of spiro-OMeTAD.

Perovskite solar cells (PSCs) are rapidly advancing as a potential alternative to conventional silicon solar cells, with their power conversion efficiency (PCE) boosted to over 25% in the last decade because of the significant progress in the optimization of the composition of the perovskite materials and development of new hole-transport materials (HTMs).[1–5] To date, the most widely used organic small molecular HTM in PSCs has been 2,2′,7,7′-tetrakis-(*N*,*N*-di-*p*-methoxyphenylamine)9,9′-spirobifluorene (spiro-OMeTAD), which exhibited a promising PCE of 25.17%.[6] Nonetheless, it suffers from a high production cost and tedious synthetic procedures. In addition, dopants like 4-*tert*-butylpyridine (*t*-BP) and lithium bis(trifluoromethanesulfonyl)imide (Li-TFSI) are needed for spiro-OMeTAD in order to obtain high device performance because of its intrinsic low hole mobility. However, hygroscopic additives will accelerate the deterioration of the perovskite, thus resulting in a decrease in the long-term device stability of the cell.[7–9] Consequently, further development of efficient and dopant-free HTMs is highly desirable.[10]

A thiophene-fused polyaromatic, cyclopenta[2,1-*b*:3,4-*b*′]dithiophene (CPDT), has been shown to have excellent charge-transport ability due to its rigid structure with an extended π-conjugation system. CPDT derivatives have been employed in organic light-emitting diodes (OLEDs), organic field-effect transistors (OFETs), and organic photovoltaic devices (OPVs).[11–13] Recently, we have demonstrated that CPDT derivatives incorporating a dithiolane ring in the central core with two triphenylamine groups can be used as HTMs in PSC fabrication, affording an impressive PCE of 19.07%, presumably owing to the intermolecular S···S interactions.[14] However, the hygroscopic dopants Li-TFSI and *t*-BP were still needed in these CPDT-based HTMs.

In this work, we report two new star-shaped CPDT-based HTMs, denoted as **T-CPDT**[15] and **C-CPDT**, based on a central CPDT core endowed with four aryl amine moieties (Fig. 1) and their application in PSCs. The difference between **T-CPDT** and **C-CPDT** is the replacement of two *p*-methoxytriphenylamine units in the central core of **T-CPDT** with two *p*-methoxydiphenylamine-substituted carbazole segments. The introduction of the carbazole groups on **C-CPDT** was found to increase the planarity of molecules, leading to the formation of a smooth and uniform thin film, and thus hole-transporting ability. More importantly, devices fabricated using the **C-CPDT** HTM without using any dopant achieved an impressive PCE of 19.68%, which is significantly higher than that of the device based on **T-CPDT** (11.45%).

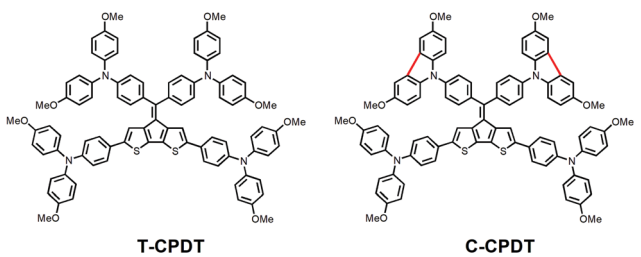

Fig. 1 Chemical structures of **T-CPDT** and **C-CPDT**.

[a] *Department of Chemical and Materials Engineering, Chang Gung University, Taoyuan 33302, Taiwan*
[b] *Division of Neonatology, Department of Pediatrics, Chang Gung Memorial Hospital, Linkou Taoyuan 33305, Taiwan*
[c] *Center for Green Technology, Chang Gung University, Taoyuan 33302, Taiwan*
[d] *Department of Chemistry, Soochow University, Taipei 11102, Taiwan. E-mail: ydlin@scu.edu.tw*
[e] *Department of Applied Chemistry, National Chiayi University, Chiayi 60004, Taiwan*
[f] *Department of Chemistry, National Central University, Taoyuan 32001, Taiwan*
[g] *Institute of Chemistry, Academia Sinica, Taipei 115024, Taiwan*

† Electronic supplementary information (ESI) available. See DOI: 10.1039/d1cc02396a

The detailed synthetic route and the NMR and mass spectra characterization of **C-CPDT** are illustrated in the ESI.† Fig. 2a shows the normalized UV-vis absorption and photoluminescence spectra of **T-CPDT** and **C-CPDT** in chlorobenzene and the corresponding data are summarized in Table 1. These CPDT-based HTMs exhibited intense absorption in the range of 300–500 nm. The maximum absorption peaks of **T-CPDT** and **C-CPDT** are centered at 413 nm and 410 nm respectively, and are attributed to the π–π* transitions. However, both HTMs showed a weak absorption band at around 540 nm, which may have resulted from the intramolecular charge transfer (ICT) transitions from the side arm triphenylamine moieties to the central CPDT core. This is supported by time-dependent density functional theory (TDDFT) calculations shown in Fig. S1 and Table S1 (ESI†). The photoluminescence spectra of **T-CPDT** and **C-CPDT** exhibited a maximum peak at 508 nm and 512 nm, respectively. An optical bandgap (E_g) of 2.70 and 2.74 eV for **T-CPDT** and **C-CPDT**, respectively, was calculated according to the normalized Uv-Vis and PL spectra. It was found that the UV and PL profiles are similar in the solution, presumably ascribable to the very small structural difference between **T-CPDT** and **C-CPDT**.

In order to gain an insight into the correlation between the molecular geometry and electronic properties, the optimized structure and frontier HOMO and LUMO of the two derivatives were simulated by density functional theory (DFT) (Fig. 2b and Fig. S2, ESI†). It was found that the two carbazole units in **C-CPDT** adopt a highly planar geometry compared with its triphenylamine counterpart (**T-CPDT**), suggesting that a close molecular packing may benefit the hole transportation between the neighboring molecules. The electron density of the HOMO mainly delocalizes over the half backbone of the molecule, while the LUMO spreads mainly on the central CPDT core. The good overlap between the HOMO and LUMO is expected to be advantageous to hole-transport ability. According to DFT calculations, the HOMO and LUMO energy levels of **T-CPDT** and **C-CPDT** were determined to be −4.16/−1.66 eV and −4.27/−2.01 eV, respectively. Thus, the E_g values of **T-CPDT** and **C-CPDT** were estimated to be 2.50 eV and 2.26 eV, respectively (Fig. 2b).

The HOMO levels of **T-CPDT** and **C-CPDT** were measured using differential pulse voltammetry (DPV) in THF solution (1.0×10^{-3} M) and the results are shown in Fig. 2c. The energy level diagrams of **T-CPDT** and **C-CPDT** are plotted in Fig. 2d. The HOMO energy levels of **T-CPDT** and **C-CPDT** were estimated to be −5.12 eV and −5.29 eV, respectively, which are more positive than the valence band of perovskite (−5.43 eV), indicating that the new CPDT-based HTMs are suitable for efficient hole extraction from the perovskite layer to HTMs. It is noted that the deeper HOMO energy level of **C-CPDT** may lead to a higher open-circuit voltage (V_{oc}) of the corresponding PSC device. On the other hand, the LUMO levels of **T-CPDT** and **C-CPDT** were determined from the HOMO and E_g values to be −2.42 and −2.55 eV, respectively. They are higher than the conduction band of the perovskite, disfavoring the undesired electron transfer from the perovskite layer to the metal electrode. However, the HOMO values obtained by DPV were consistent with the calculated values from DFT results. We also measured the solid-state ionization potential (I_p) values of **T-CPDT** and **C-CPDT** on thin films using photoelectron spectroscopy in air (PESA), whose results are shown in Fig. S3 (ESI†). The I_p values of **T-CPDT** and **C-CPDT** were estimated to be −4.95 and −5.03 eV, respectively, which exhibit the same trend as that of oxidation potential data obtained from DPV and DFT calculations.

To explore the hole-transport abilities of **T-CPDT** and **C-CPDT** with respect to spiro-OMeTAD, hole-only devices with the structure of ITO/PEDOT:PSS/HTM/Au were fabricated to determine the hole mobility by the space-charge-limited current (SCLC) method (Fig. S4, ESI†). Under the identical conditions, the hole mobility of pristine **T-CPDT** and **C-CPDT** was estimated to be 2.37×10^{-4} and 4.39×10^{-4} cm^2 V^{-1} s^{-1}, respectively, indicating that the incorporation of a carbazole unit in **C-CPDT** indeed improves the hole mobility, due to the strong π–π stacking and thus enhanced intermolecular interactions caused by a coplanar carbazole moiety. The hole-mobility of doped spiro-OMeTAD is also recorded (2.30×10^{-4} cm^2 V^{-1} s^{-1}) using the same measurement method.

The steady-state photoluminescence (PL) and time-resolved photoluminescence (TRPL) spectra were also measured to evaluate the hole-extraction capabilities of the CPDT-based HTMs. As illustrated in Fig S5 (ESI†), it is clear that significant quenching of PL intensity was observed when HTMs were deposited on top of the perovskite layer. $MAPbI_3$/**C-CPDT** showed more quenching in PL intensity than $MAPbI_3$/**T-CPDT**, suggesting that the former HTM exhibited better hole extraction capability at the interface of the bilayer. In addition, the hole transport properties were further validated by TRPL experiments. From the TRPL decay profile, the perovskite/HTM bilayer exhibited a much fast time decay, much shorter than those of the pristine perovskite layer.

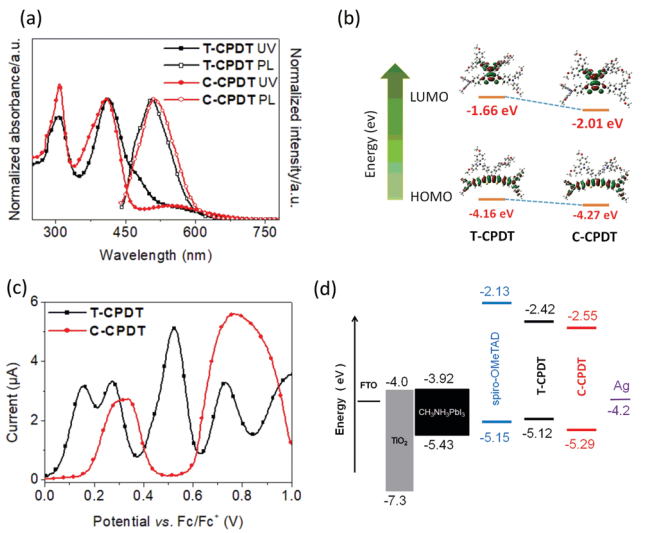

Fig. 2 (a) Normalized absorption and photoluminescence spectra of **T-CPDT** and **C-CPDT** in chlorobenzene solution. (b) The electron densities of HOMO and LUMO levels of **T-CPDT** and **C-CPDT** calculated by DFT at the B3LYP/6-31(d,p) level. (c) Differential pulse voltammetry (DPV) of **T-CPDT** and **C-CPDT** in THF solution. (d) Energy level diagrams of **T-CPDT** and **C-CPDT** used in perovskite solar cells.

Table 1 Photophysical and electrochemical data of **T-CPDT**, **C-CPDT** and spiro-OMeTAD

HTM	λ_{abs}[a] (nm) ($\varepsilon \times 10^{-4}/M^{-1}$ cm^{-1})	λ_f[a] (nm)	E_{HOMO}[b] (eV)	E_{0-0}[c] (eV)	E_{LUMO}[d] (eV)	I_p[e] (eV)	E_{HOMO}[f] (eV)	E_{LUMO}[f] (eV)
T-CPDT	413 (8.26)	508	−5.12	2.70	−2.42	−4.95	−4.16	−1.66
C-CPDT	410 (7.09)	512	−5.29	2.74	−2.55	−5.03	−4.27	−2.01
spiro-OMeTAD	389 (18.37)	428	−5.15	3.02	−2.13	−4.98	−4.21	−0.61

[a] Maximum of the absorption and fluorescence bands in chlorobenzene solution. [b] Determined by differential pulse voltammetry. [c] The value of E_{0-0} was obtained from the intersection of normalized absorption and photoluminescence spectra. [d] Energy of the LUMO of the compounds estimated by $E_{HOMO} + E_{0-0}$. [e] Ionization potential was measured by the photoemission in the air method from films. [f] TDDFT/B3LYP/6-31G(d,p) level calculated values.

The lifetimes of **T-CPDT** and **C-CPDT** deposited on the perovskite film were estimated to be 21.39 and 16.57 ns, respectively, which are shorter than that of the pristine perovskite film (31.78 ns), indicating that **C-CPDT** has better hole extraction ability than **T-CPDT** (Table S2, ESI†). These results are consistent with that obtained from SCLC experiments.

In addition to the hole transport properties, the morphological properties of the HTM films on the surface of the perovskite layer also played a key role in the device performance. The morphology of perovskite films coated with **T-CPDT** and **C-CPDT** was examined using scanning electron microscopy (SEM). As shown in Fig. S6 (ESI†), the top-view SEM images of **T-CPDT** and **C-CPDT** present a homogeneous and fully covered layer on top of the perovskite film. The surface roughness of the perovskite with HTMs was studied by atomic force microscopy (AFM). The root-mean-square (RMS) roughness values of **T-CPDT** and **C-CPDT** are 11.53 and 8.29 nm, respectively (Fig. S7, ESI†). Apparently, **C-CPDT** showed smoother and more uniform film coverage on the perovskite surface. The better uniformity of **C-CPDT** may have likely resulted from the better planarity of carbazole units on the structure.

To exploit the potential of **T-CPDT** and **C-CPDT** as dopant-free HTMs in PSCs, a device structure of FTO/c-TiO_2/mp-TiO_2/$CH_3NH_3PbI_3$/HTM/Ag was fabricated. The details of the fabrication process can be found in the ESI.† For parallel comparison, the device with spiro-OMeTAD as a HTM was also prepared as a reference using the same fabrication procedure. A cross-section SEM image of the complete device with the **C-CPDT** HTM is shown in Fig. S8 (ESI†). The typical photocurrent density–voltage (*J–V*) characteristics based on dopant-free **T-CPDT**, **C-CPDT**, and doped spiro-OMeTAD are shown in Fig. 3a. The corresponding photovoltaic parameters are summarized in Table 2. The devices based on **T-CPDT** gave a poor PCE of 11.45%, an open-circuit voltage (V_{oc}) of 0.88, a short-circuit density (J_{sc}) of 21.37 mA cm^{-2} and a fill factor (FF) of 60.9%. In contrast, the optimized PSCs based on **C-CPDT** as the HTM exhibited a promising PCE of 19.68%, together with a V_{oc} of 1.14 V, a J_{sc} of 23.27 mA cm^{-2}, and an FF of 74.2%, which are superior to those of the device using doped spiro-OMeTAD (V_{oc} = 1.09 V, J_{sc} = 23.42 mA cm^{-2}, FF = 75.5%, and PCE = 19.27%). The device with **C-CPDT** showed a significantly improved PCE compared to that with **T-CPDT**, which could be ascribed to the higher hole mobility, a better film-forming property and strong hole-extraction capability. A near coplanar structure by fusing the carbazole moiety on **C-CPDT** is suggested to have a contribution. Fig S9 and Table S3 (ESI†) show a small hysteresis between the forward and reverse scans for the **C-CPDT**-based device. The corresponding incident photon-to-electron conversion efficiency (IPCE) spectra are depicted in Fig. 3b. The integrated photocurrents of devices with undoped **T-CPDT**, **C-CPDT**, and doped spiro-OMeTAD are 21.16, 22.97 and 23.08 mA cm^{-2}, respectively, which are in good agreement with the J_{sc} values measured in *J–V* scanning. The stable power output was measured at the maximum power point (MPP) to further verify the measured PCEs from the *J–V* curves for the devices based on **T-CPDT** and **C-CPDT** up to 300s (Fig. 3c). The **T-CPDT**- and **C-CPDT**-based devices exhibited reliable PCEs of 19.52% and 11.03%, respectively. Fig. 3d shows an average PCE value of 18.82% with a narrow distribution for devices based on **C-CPDT**, compared to that of **T-CPDT**-based devices (9.88%). These results indicate good reproducibility of the data for the devices made from **C-CPDT**.

The long-term stability of PSC devices based on undoped **T-CPDT** and **C-CPDT**, and doped spiro-OMeTAD was further studied in ambient air without encapsulation, with a relative humidity of around ~40% at a temperature of 20–25 °C in the dark.

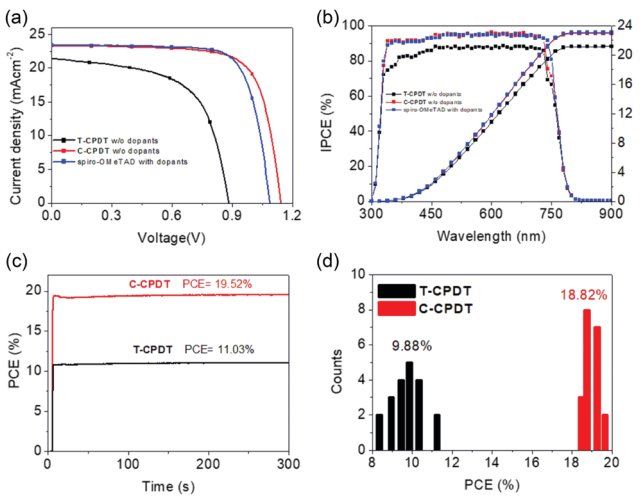

Fig. 3 (a) *J–V* curves, (b) IPCE spectra of the best-performing PSCs, (c) stable output PCE measured as a function of illumination time and (d) statistical efficiency histograms of PCEs with different HTMs.

Table 2 Photovoltaic parameters of the best-performing PSCs with dopant-free **T-CPDT** and **C-CPDT** and doped spiro-OMeTAD as HTMs

HTM	V_{oc} [V]	J_{sc} [mA cm^{-2}]	FF (%)	PCE_{max} [%]
T-CPDT	0.88	21.37	60.9	11.45
C-CPDT	1.14	23.27	74.2	19.68
Spiro-OMeTAD	1.09	23.42	75.5	19.27

As shown in Fig. S10 (ESI†), the PSCs with spiro-OMeTAD showed a much faster degradation than those with the CPDT series. The presence of hydrophilic dopants is suggested to be the cause. It can be noted that **C-CPDT**-based PSCs exhibited better stability than **T-CPDT**-based ones. This may result from the more hydrophobic nature based on the measurement of water-contact angles (in the inset of Fig. S10, ESI†).

In summary, we have developed a highly efficient hole-transport material **C-CPDT**, whose two carbazole units induce a near planar molecular geometry for better packing, which in turn may result in a higher hole mobility, better hole extraction ability and improved thin-film morphology compared with the counterpart carrying a non-planar triphenylamine moiety. Therefore, the PSC device based on **C-CPDT** without dopants exhibited a remarkable PCE of 19.68%, which is higher than that of the reference cell based on doped spiro-OMeTAD (19.27%). It also exhibited excellent long-term stability compared to the reference cell.

Y.-D. Lin is thankful for the support from the Ministry of Science and Technology (Grant Number MOST 109-2113-M-031-007). K.-M. Lee is thankful for the support from the Ministry of Science and Technology, Taiwan (Grant Number MOST 108-2628-E-182-003-MY3), Chang Gung University (QZRPD181) and Chang Gung Memorial Hospital, Linkou, Taiwan (CMRPD2J0041). We greatly appreciate Professor Y.-T. Tao at the Institute of Chemistry, Academia Sinica, for assistance in water contact angle measurements.

Conflicts of interest

There are no conflicts to declare.

Notes and references

1 A. Kojima, K. Teshima, Y. Shirai and T. Miyasaka, *J. Am. Chem. Soc.*, 2009, **131**, 6050–6051.
2 NREL, Best Research-Cell Efficiency Chart, https://www.nrel.gov/pv/cell-efficiency.html, accessed: May 2021.
3 Y. Han, H. Zhao, C. Duan, S. Yang, Z. Yang, Z. Liu and S. F. Liu, *Adv. Funct. Mater.*, 2020, **30**, 1909972.
4 S. Yang, W. Liu, Y. Han, Z. Liu, W. Zhao, C. Duan, Y. Che, H. Gu, Y. Li and S. F. Liu, *Adv. Energy Mater.*, 2020, **10**, 2002882.
5 C. Duan, J. Chi, M. Zhang, Y. Han, S. Yang, H. Zhao, H. Bian, J. Yao, K. Zhao, Z. Liu and S. F. Liu, *Adv. Energy Mater.*, 2020, **10**, 2000691.
6 M. Jeong, Y. Cho, B. Lee, S. Jeong, C. Yang, I. W. Choi, M. Kim, Y. Jo, H. W. Choi, D. S. Kim, I. W. Choi, J.-H. Bae, E. M. Go, J. Lee and S. K. Kwak, *Science*, 2020, **369**, 1615–1620.
7 W. Deng, X. Liang, P. S. Kubiak and P. J. Cameron, *Adv. Energy Mater.*, 2018, **8**, 1701544.
8 Q. Ge, J. Shao, J. Ding, L. Deng, W. Zhou, Y. Chen, J. Ma, L. Wan, J. Yao, J. Hu and Y. Zhong, *Angew. Chem., Int. Ed.*, 2018, **57**, 10959–10965.
9 C. Shen, Y. Wu, H. Zhang, E. Li, W. Zhang, X. Xu, W. Wu, H. Tian and W. Zhu, *Angew. Chem., Int. Ed.*, 2019, **58**, 3784–3789.
10 H. Guo, H. Zhang, C. Shen, D. Zhang, S. Liu, Y. Wu and W.-H. Zhu, *Angew. Chem., Int. Ed.*, 2021, **60**, 2674–2679.
11 R. P. Ortiz, A. Facchetti, T. J. Marks, J. Casado, M. Z. Zgierski, M. Kozaki, V. Hernández and J. T. L. Navarrete, *Adv. Funct. Mater.*, 2009, **19**, 386–394.
12 Z. Fei, X. Gao, J. Smith, P. Pattanasattayavong, E. B. Domingo, N. Stingelin, S. E. Watkins, T. D. Anthopoulos, R. J. Kline and M. Heeney, *Chem. Mater.*, 2013, **25**, 59–68.
13 M. Zhang, Y. Wang, M. Xu, W. Ma, R. Li and P. Wang, *Energy Environ. Sci.*, 2013, **6**, 2944–2949.
14 Y.-D. Lin, K.-M. Lee, S. H. Chang, T.-Y. Tsai, H.-C. Chung, C.-C. Chou, H.-Y. Chen, T. J. Chow and S.-S. Sun, *ACS Appl. Energy Mater.*, 2021, **4**, 4719–4728.
15 A. Abudulimu, R. Sandoval-Torrientes, I. Zimmermann, J. Santos, M. K. Nazeeruddin and N. MartÍn, *J. Mater. Chem. A*, 2020, **8**, 1386–1393.

